GlueX-doc-1789
SVN: docs/GlueXdoc/photon_detection_efficency
Draft: June 30, 2011
Original: July 15, 2011

Studies on photon detection efficiency in the transition region from BCAL to FCAL

B. Zihlmann

Abstract

We studied the photon detection efficiency in the transition region from BCAL to FCAL by generating single photons from the target center and ± 10cm from the target center between 7 and 22 degrees. The Monte Carlo simulation includes a newly implemented geometry with a realistic modeling of the BCAL readout that has a cooling system for the silicon photo detectors. This cooling system has a central massive copper plate covering all readout elements of the BCAL and adding substatial material to photon trajectories that pass though this section of the detector going into the FCAL. It is found that with the current geometrical detector setup there is an inefficiency gap between BCAL and FCAL of about 1.5 degrees. Replacing the copper material of the cooling plate for the BCAL readout by aluminum has only a small impact on the depth of the gap. However, moving the most downstream FDC package upstream by 20cm will reduce this gap substantially down to about 1.0 degree.

1 Introduction

In order to study the photon detection efficiency, Monte Carlo data have been generated where single photons are simulated emanating from three different vertex positions 0 cm and ± 10cm from the target center. The energy range is 0.1 GeV to 3.0 GeV while the polar angle covers the range from 7 to 21 degree. The azimuthal angle is uniform from 0 to 360 degree. For each data sample 2 million events are generated. Figure 1 shows the current nominal geometry with the 4 FDC packages in the forward region, the FDC cables running upstream and a first design of the BCAL cooling system with a massive copper cooling plate. A 10 degree trajectory from the target center will pass right through the last FDC package frame and will miss the BCAL readout system. This will be a source of inefficiency for detecting photons as the frame at this location is reinforce with solid G10. At increasing angles the trajectory will pass through the BCAL readout where the thick copper cooling plates and aluminum casing will provide substantial material to cause a photon to shower. Because the FCAL is much further downstream, a photon that started a shower in this regions will most likely not be reconstructed properly.

2 Photon detection

The photon detection efficiency is determined as follows: First, the generated energy is plotted against the reconstructed photon energy separately for the FCAL and BCAL reconstructed photons. In this plot all reconstructed photons are used, which potentially can be larger than one. The binning steps of this histogram was set to be 0.05 GeV in energy and 0.083 degree

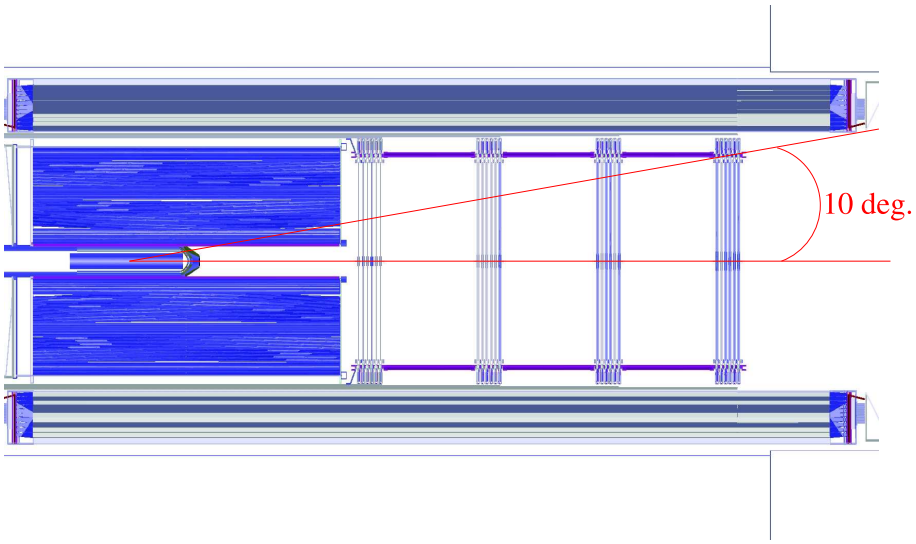

Figure 1: Side view of the detector geometry with a 10 degree trajectory from the target center.

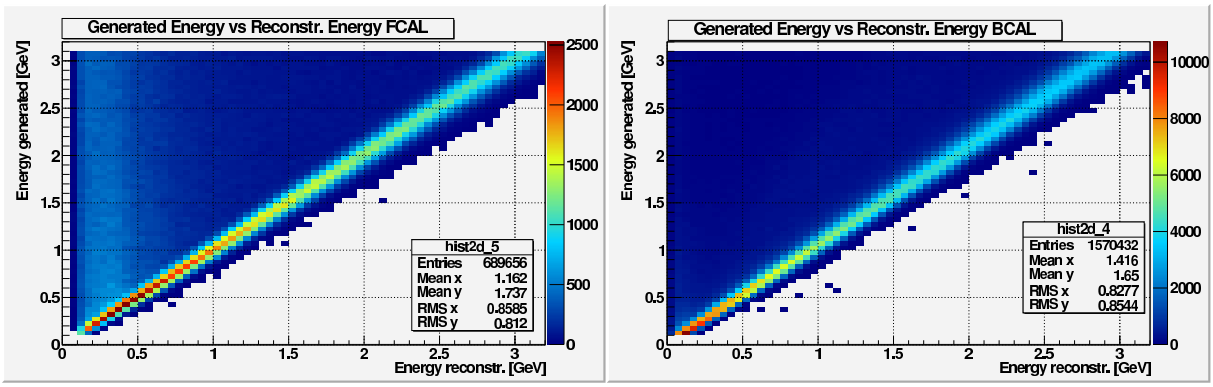

Figure 2: Generated versus reconstructed photon energy for FCAL (left) and BCAL (right).

in angle. Note that in the case of the FCAL (see Fig.2) there is an enhancement of low energy photons being reconstructed for all generated photon energies. This is an artefact of the reconstruction algorithm where the shower in the FCAL is split up into more than one separate cluster leading to several low energetic photons rather than one high. It is also evident that the slope of the ridge is not the same for the FCAL and the BCAL ridge is not diagonal meaning the reconstructed energy in the BCAL is slightly underestimated.

For each bin in generated photon energy the 2-dim histogram is projected to the horizontal axis and the resulting 1-dim histogram in reconstructed energy is fit with a Gaussian function to determine the peak position and its width. This will constitute the mean reconstructed energy and sigma of the generated photon energies of that energy bin. In the same way this is also done for the generated and reconstructed polar angles. For both the FCAL and BCAL the generated angle versus reconstructed angle is shown in Figure 3. While there is again a good correspondence between generated and reconstructed angle there is a fuzziness in the transition region between FCAL and BCAL. While this can not be readily identified in these

histograms it is seen much more pronounced in the 1-dimensional projections of the bins to the horizontal axis. What can not be seen in these plots because they are dominated by the ridge is that there are a non negligible number of events at angles larger than 10.5 degree in the case of the FCAL and at angels lower than 10.5 degree in the case of the BCAL. The cause and effect of these hits will be discussed later as they will show up as small efficiencies for the FCAL and BCAL in a region not physically covered by the individual detectors.

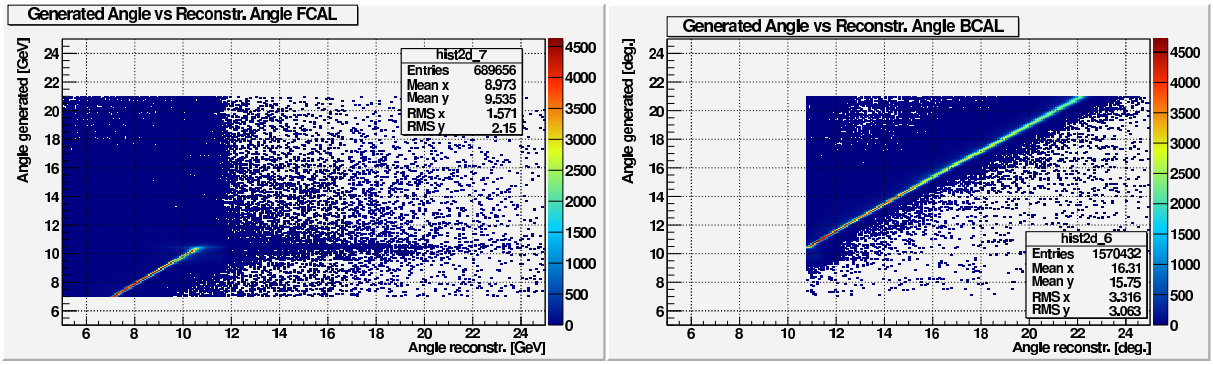

Figure 3: Generated versus reconstructed angle for FCAL (left) and BCAL (right).

A generated photon is considered to be reconstructed properly if the reconstructed energy is within $\pm$ 3 σ of the mean reconstructed energy for that generated energy bin and at the same time fulfills the same requirement for the polar angle. This selection is made relative to reconstructed quantities so that they will not be biased by an insufficient energy and angle calibration. The reconstruction efficiency in a given generated energy bin of photons is the ratio of reconstructed photons for that bin divided by the generated number of photons in that bin. This efficiency is calculated as a function of generated photon energy and as a function of generated polar angle.

For completeness the results of the fits to determine the mean reconstructed energy and angle as well as their width is shown in figure 4 separately for FCAL and BCAL. While the geometrical coverage of the FCAL only covers angles up to about 10.5 degree there are still fit results far beyond that angle. This is because in a non negligible amount of events some spray of particles emanating from the BCAL will hit the FCAL preferentially hitting the perifery of it resulting in a broad bump at larger angles. The further upstream in the BCAL the spray is generated, the further inwards to the FCAL the hit is recorded while the width of the energy distribution of these hits is very large as indicated by the sharp rise of σ in the top right plot on the right. The BCAL on the other hand can see hits at more forward angles than it geometrically covers because photons that would otherwise directly go into the FCAL start to shower in the frame of the last FDC package or the BCAL readout and some back splash of particles hit the detector. Again as in the case of the FCAL it will result in a broad bump as represented by the large *sigma* given by the fit.

3 Efficiency

The photon detection efficiency is determined by the ratio of reconstructed photons within the cuts of energy and angle divided by the generated number of photons for a given energy

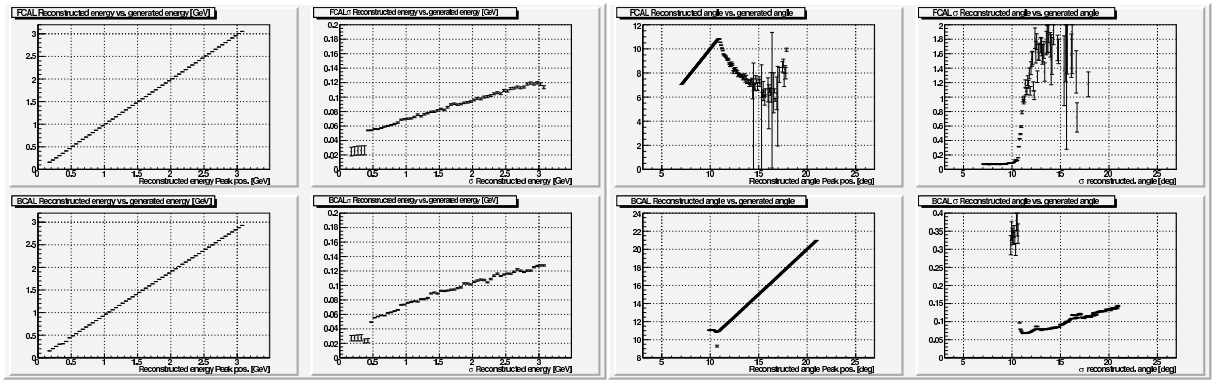

Figure 4: Fit results for the mean energy and width as a function of generated energy for both FCAL and BCAL (left) and the same for the generated angles (right).

and angle bin. For this reason the efficiency is not represent a traditional detector efficiency, it includes a geometrical acceptance aspect and material budget along the path of the photon as well.

Because of the large number of bins in energy and angle the amount of histograms and plots is huge. Rather than generating an whole encyclopedia of plots a graphical user interface (GUI) based on ROOT has been created to brows through the numerous plots as a function of bins in angle and energy. There are in total 64 energy bins and 240 angle bins for three different target vertex positions. At this point the whole analysis sequence is given as an itemized list for clarity.

- hdgeant: generate 2M Monte Carlo events. $0.1GeV < E < 3.0GeV$, $7° < \theta < 21°$
- mcsmear: smearing of the MC data.
- hd_ana: analyze MC data with a plug-in to generate ROOT tree of photons.
- pandf: analyze ROOT tree to create efficiency plots.
- scaner: GUI to view and brows the efficiency plots.

The basic idea of the GUI is to facilitate browsing the photon detection efficiency plotted as a function of energy or angle while selecting the angle bin and energy bin respectively. The GUI provides additional selection criteria based on target vertex position (center and $\pm$ 10cm) and geometry. The geometry is either the normal standard geometry where all 4 FDC packages are positioned equidistant in the bore of the magnet or where the fourth FDC package is moved 20 cm further upstream so that the FDC frame of that package is aligned with the BCAL readout for trajectories emanating from the target center and pass through the BCAL readout area.

As an example of the GUI a screen shot is shown in figure 5. In this particular case the modified geometry is chosen with the generated photon energy set at 1 GeV and the efficiency is plotted as a function of the polar angle. The FCAL data is plotted in red while the BCAL data is plotted in black. The gap between the FCAL and the BCAL is clearly visible as the detection efficiency drops to basically zero. What is also seen is two dips in the efficiency at 12.5 and 16 degree. These are caused by the frames of the FDC package number three and two respectively. The error bars are not calculated correctly at this point and represent an overestimation of the true errors.

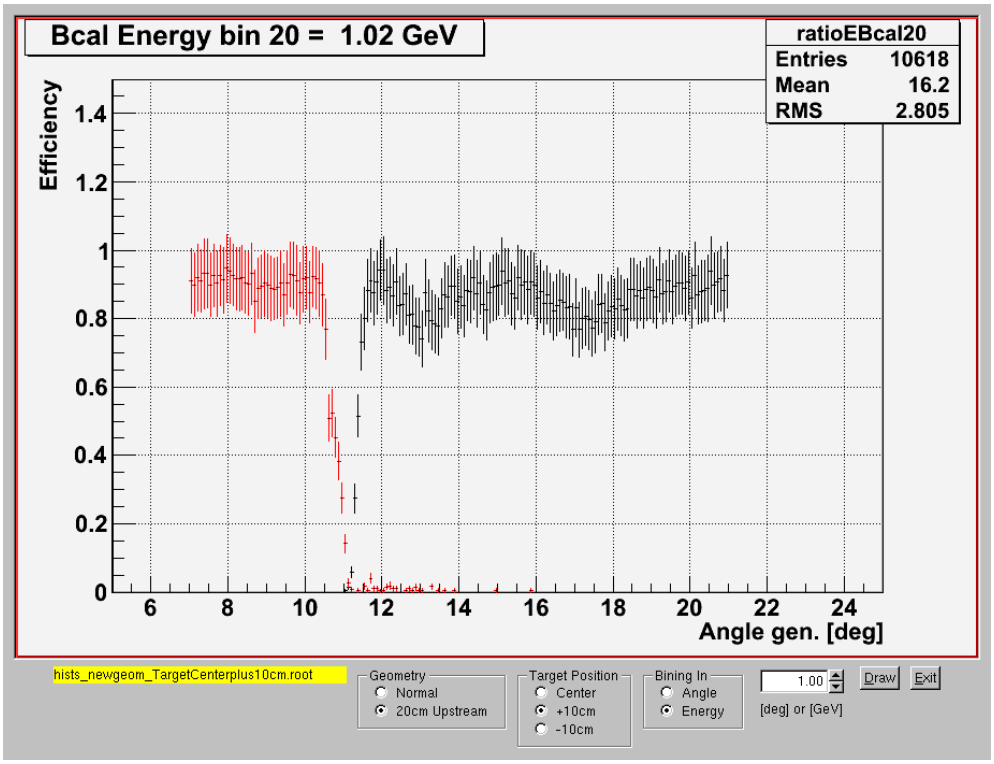

Figure 5: Screen shot of the GUI to browse the photon detection efficiency data. See text for more detail.

3.1 Energy dependence of the photon detection efficiency

Looking at the photon detection efficiency as a function of energy for any angel other than the gap region is very flat in case of the FCAL with the exception at energies below 0.5 GeV. At these small energies the efficiency continuously drops (see fig. 6). This is because the energy resolution gets worse and photon energy depositions drop below the energy cut and get lost in the reconstruction. This gets more severe the smaller the initial photon energy is. The same situation applies to the BCAL, the efficiency is flat above 0.5 GeV but then drops significantly. However there is an additional twist for angles in the dip regions of 12.5 and 16 degree. At the two angles referred to as the dip region, the efficiency starts to drop slightly already at 1.5 GeV and continues to drop more towards lower energies. This is because the photon can start to shower already in the frame of the FDC and some of the energy can get lost and is not seen by the BCAL or the shower clusters are not added up correctly to one single photon shower but rather split up into several lower energy photon showers. Generally the photon detection efficiency is reasonably high at about 90% for energies larger than 0.5 GeV and all angles but the dip regions. Note that there is some efficiency data from the FCAL in the angular region beyond its acceptance (right plot of figure 7 5). This is caused by back splashes in the BCAL, where part of the shower or a single sufficiently high energetic lepton or photon of the developing shower escapes the BCAL volumen and propagtes forward into the FCAL as mentioned above in section 2. While these efficiency data points should not be regarded as genuine photon detection efficiencies they have been left in the plots as a reminder of this effect and serves as a measure of the frequency with which they may occure.

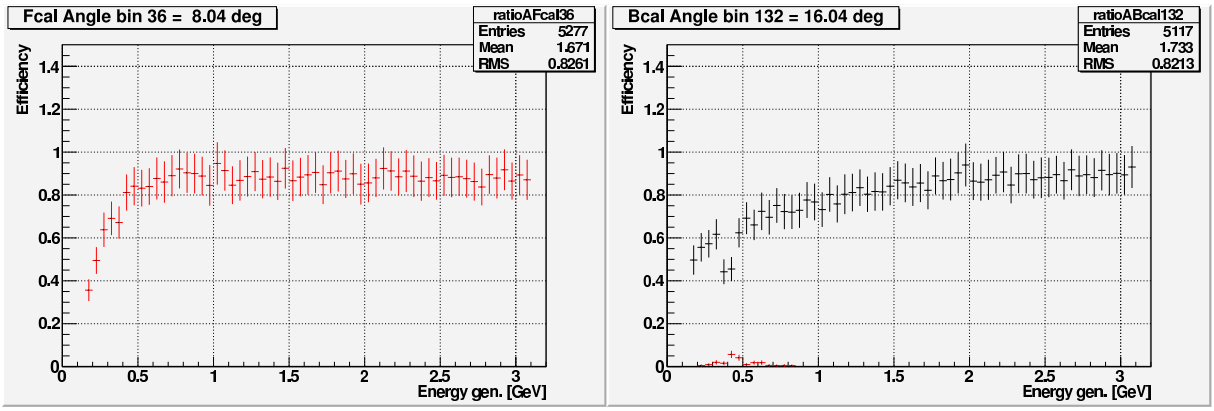

Figure 6: Photon detection efficiency as a function of energy for the FCAL at 8 degree (left) and the BCAL at 16 degree dip region (right). The FCAL data is in red the BCAL data is in black.

The additional information from the FCAL in such events will compensate for some of the missing reconstructed energy but will have a potential bias on the reconstructed the missing momentum in a specific direction of the polar angle θ.

3.2 Angular dependence of the photon detection efficiency

The angular dependence of the photon detection efficiency has a very rich structure. This is shown in figure 7 where the detection efficiency is plotted as a function of angle for 1 GeV photons. In black is the BCAL data and in red is the FCAL data. One can clearly see a dramatic drop of the efficiency to basically zero at the angle of 10.5 degree. The drop is very sharp when approaching the gap from larger angles (black points). The gap has a richer structure when approaching it from lower angles (red points). Looking at the left plot in figure 7 the drop in efficiency starts in the FCAL at an angle of about 9.6 degree and drops fast to below 60% at an angle of about 10.0 degree. At this point the efficiency stays constant or even recovers a little bit before dropping sharply again at about 10.6 degree and finally going to zero at 10.9 degree. The total gap width is about 1.7 degree starting from 9.6 degree and recovering at 11.3 degree. The initial drop to below 60% starting at 9.6 degree is caused by the frame of the last FDC package while the drop to virtually zero is caused by the heavy readout system of the BCAL.

Depending on the vertex position in the target the angular position of the gap moves. Also the features of the gap in particular the effect of the last FDC package frame does change a little while the gap width stays almost the same. As can be seen in figure 7 changing of the vertex position by 10 cm upstream will move the start of the gap by 0.3 degree from 9.6 to 9.3 degree while moving the end of the gap from 11.3 degree to about 10.9 degree.

Similarly the two dip regions in the BCAL at around 12.5 and 16 degree will shift to larger angles when the vertex in the target is moved upstream. These dips will move to smaller angles when the vertex at the target is moved down stream (not shown).

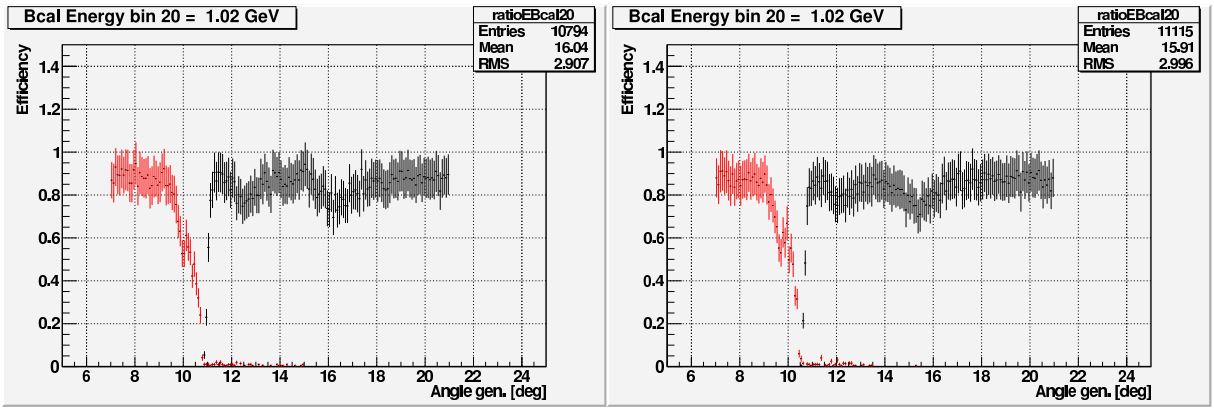

Figure 7: Photon detection efficiency as a function of angle for 1 GeV photons generated at the target center (left) and 10 cm further upstream stream in the target (right).

3.3 Copper vs. Aluminum

To test the impact of the massive copper cooling plate on the photon detection efficiency the MC geometry of the BCAL readout has been minimally modified by replacing the copper material by aluminum. Because the geometry is not changed at all the effect of the material itself can be assessed. In figure 8 a comparison is shown between a copper cooling plate and an aluminum cooling plate. The efficiency is plotted as a function of polar angle for photon energies of 1 GeV. Here the photons were generated from the target center. There is a clear distinct difference between these two simulations. While the efficiency at small angles drops sharply in both cases it recovers somewhat in the case of the aluminum material before dropping to zero entirely. While the use of aluminum cannot prevent the drop to zero it has an impact on the apparent width of that drop to zero.

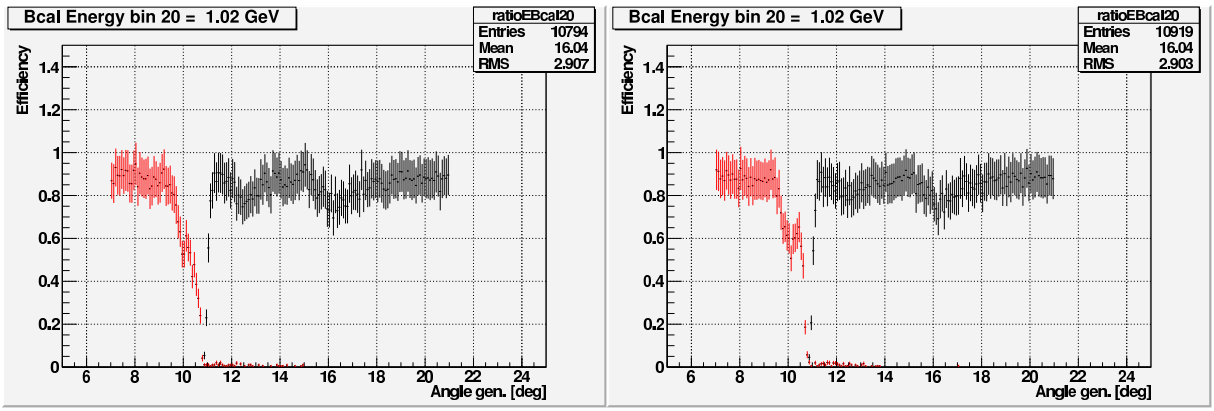

Figure 8: Photon detection efficiency as a function of angle for 1 GeV photons generated at the target center with a copper cooling plate (left) and an aluminum cooling plate (right).

For completeness similar comparison plots are shown in the appendix in figure 10 and 11. Regardless of the target vertex position the initial drop in efficiency at small polar angle recovers slightly before dropping entirely to zero. The main difference due to the vertex

position is that the location of the gap moves while the main structural features of the gap itself stay mostly the same and are mainly determined by the detector geometry like the BCAL readout and the FDC frames.

3.4 Geometry considerations

In order to test if the width of the gap region can be reduced by optimizing the position of the detectors the last FDC package was moved 20 cm further upstream in the geometry. This move will align the frame of the FDC package with the BCAL readout for trajectories from the target center. The results are shown in figure 9 for photons generated at the target center and photons generated 10 cm further upstream. On can clearly see that the structure of the gap has changed. In particular the initial drop in efficiency in the FCAL starts at larger angles. For the central target vertex position the drop starts at about 10.2 degree reducing the total width of the gap by about 0.5 degree to 1.1 degree. A similar effect is seen for photons generated 10 cm further upstream in the target. In this case the little step around 10.7 degree at 50% efficiency caused by the FDC frame is still visible.

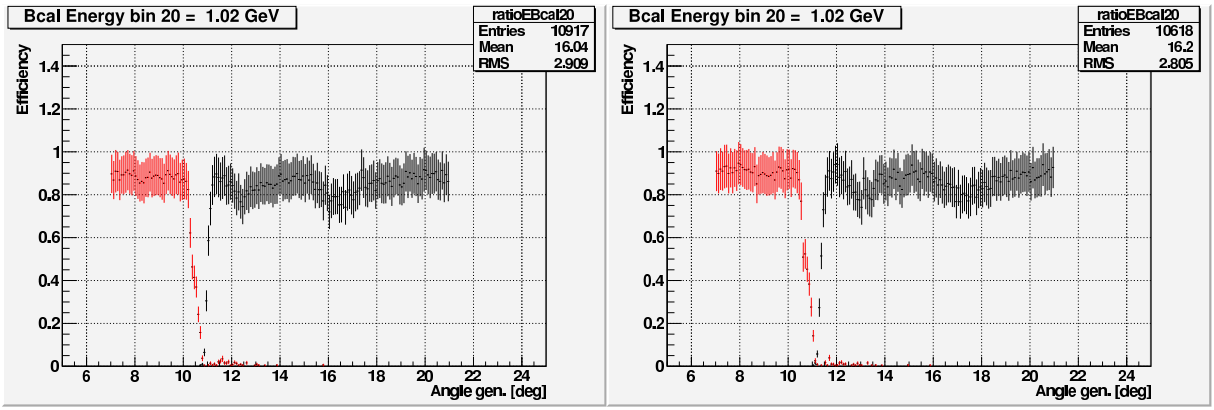

Figure 9: Photon detection efficiency as a function of angle for 1 GeV photons generated at the target center (left) and 10 cm further upstream stream in the target (right) for the new geometry where the last FDC package has been moved upstream by 20 cm.

3.5 Photon detection losses in the FDC frames.

A detailed inspection of the dip regions around 12 and 16 degree where the efficiency is reduced reveals several points. First of all these dips are caused by the frames of the FDC package three and two respectively. Trajectories from the target pass right through the frames of these FDC packages before hitting the BCAL. In particular in the region where the individual FDC planes are bolted together the frame material is solid G10 to provide sufficient stiffness for the O-rings to seal off the detector gas volume. This additional material will cause some photons to shower and the magnetic field will spread out this initial shower particles over sufficiently large azimuthal angles, such that this initial single photon will be reconstructed as two or more lower energy photons or even part of the energy gets lost entirely. Notices that the exact location of the minimum of these dips in polar angles shift depending on the vertex position in the target. This is of course expected, however if one looks at the energy dependence of the

efficiency in area of these dip regions two important issues can be observed. See also figure 6 right plot where the efficiency in the BCAL is shown at 16 degree polar angle as a function of photon energy. The efficiency is constant and flat above 2 GeV. It degrades however as the energy decreases and this degradation becomes more severe as the energy gets smaller.

First, the efficiency is not flat anymore as a function of energy but rather has a positive slope increasing as the photon energy increases and reaching a plateau around 1.5 GeV. This slope is steeper the closer the polar angle is to the center (minimum) of the dip. The efficiency hardly degrades for photon energies of 2 GeV and more in this regions. However the lower the photon energy the stronger the degradation.

Secondly, the actual dip region is larger than it appears when looking at the angular distribution at a fixed photon energy. Looking at the efficiency as a function of energy at the edge of the dip region one notices a significant reduction in efficiency for detecting photon at energies below 1 GeV. Because the statistics becomes dominated by the higher energy photons the effect is small when looking at the angular distribution of the efficiency average over all energies. Only when looking at the energy dependence one notices the diminished efficiency at low photon energy. As a result the dip becomes more pronounced and wider with lower photon energy.

These dip regions become less and less pronounced with in creasing photon energy. At 1.5 GeV the dip region around 12 degree has basically vanished while the one around 16 degree is only marginally visible. At photon energies of 2 GeV no dip regions is discernible anymore within statistics.

4 Analysis code

The analysis code and the final root data files to scan the histograms together with the GUI can be found in the repository and retrived like this:

```
svn checkout https://halldsvn.jlab.org/repos/trunk/home/zihlmann/photonstudy
```

5 Appendix of plots

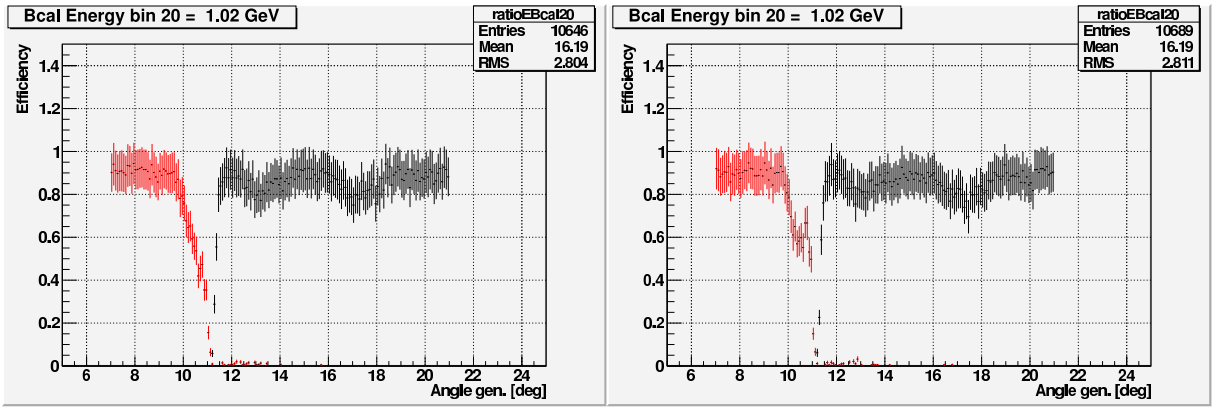

Figure 10: Photon detection efficiency as a function of angle for 1 GeV photons generated at 10 cm downstream of the target center with a copper cooling plate (left) and an aluminum cooling plate (right).

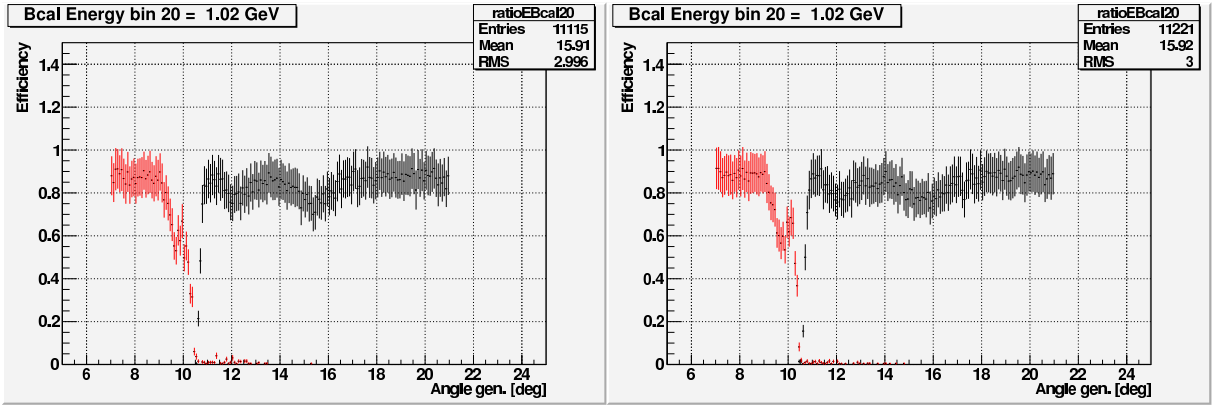

Figure 11: Photon detection efficiency as a function of angle for 1 GeV photons generated at 10 cm upstream of the target center with a copper cooling plate (left) and an aluminum cooling plate (right).